ACS OMEGA

http://pubs.acs.org/journal/acsodf

Article

Hydrogen-Bonding Interactions of 8-Substituted Purine Derivatives

Published as part of the ACS Omega virtual special issue "Nucleic Acids: A 70th Anniversary Celebration of DNA".

Zuzana Osifová, Michal Šála, and Martin Dračínský*

Cite This: *ACS Omega* 2023, 8, 25538−25548

Read Online

ACCESS | Metrics & More | Article Recommendations | Supporting Information

ABSTRACT: Hydrogen bonding between nucleobases is a crucial noncovalent interaction for life on Earth. Canonical nucleobases form base pairs according to two main geometries: Watson−Crick pairing, which enables the static functions of nucleic acids, such as the storing of genetic information; and Hoogsteen pairing, which facilitates the dynamic functions of these biomacromolecules. This precisely tuned system can be affected by oxidation or substitution of nucleobases, leading to changes in their hydrogen-bonding patterns. This paper presents an investigation into the intermolecular interactions of various 8-substituted purine derivatives with their hydrogen-bonding partners. The systems were analyzed using nuclear magnetic resonance spectroscopy and density functional theory calculations. Our results demonstrate that the stability of hydrogen-bonded complexes, or base pairs, depends primarily on the number of intermolecular H-bonds and their donor−acceptor alternation. No strong preferences for a particular geometry, either Watson−Crick or Hoogsteen, were found.

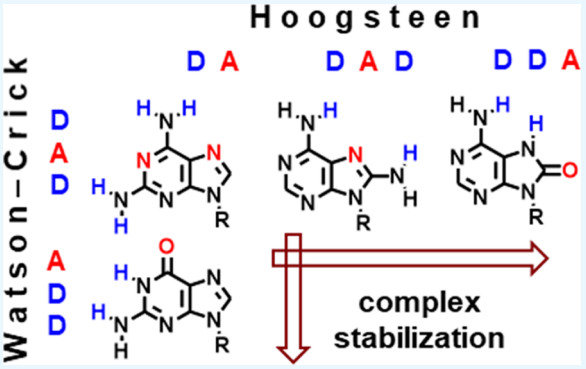

INTRODUCTION

Hydrogen bonding is indisputably one of the most important noncovalent interactions for the structure of matter and life on Earth. Although about an order of magnitude weaker than covalent bonds, hydrogen bonds (or H-bonds) determine the structure and function of large biomolecules such as proteins and nucleic acids. A hydrogen bond is an attractive interaction between a H-bond donor (D, e.g., N−H or O−H group) and a H-bond acceptor (A, e.g., N or O atom).

Nucleic acids (NAs) play essential roles in creating, encoding, transmitting, expressing, and storing genetic information in every living cell. These functions are controlled by specific intermolecular bonding abilities between nucleobases. The structures of canonical base pairs were first described by Watson and Crick in 1953,[1] bringing H-bonding to the forefront of scientific attention. Soon after that, in 1959, Karst Hoogsteen discovered an alternative base pairing. In this model, the purine base is flipped 180° (*anti*-conformation of the *N*-glycosidic bond), offering nitrogen in position 7 for interaction with its pyrimidine counterpart[2] (Figure 1). Hoogsteen base pairs were later found to occur in DNA multiplexes[3−7] as well as in DNA complexes with proteins[8] and antibiotics.[9] These findings helped to form a general concept that Watson−Crick base pairs contribute to the static functions of NAs, such as storing genetic information, while Hoogsteen base pairs enable the dynamic functions of these biomacromolecules.

In NAs, the formation of base pairs is affected by a number of factors including stacking of nucleobases, hydrogen bonding, NA conformation, interactions with counterions, and hydration.[5,10−12] The preferred interactions in NAs can thus be different from those observed for free nucleobases. For example, adenine tends to form a Hoogsteen-like complex with thymine in solution[13] and crystal,[14] indicating greater stability of this geometry. The thermodynamic stability of hydrogen-bonded complexes is dependent on the hydrogen-bond count between counterparts. For example, the Watson−Crick-like G−C base pair is more stable than the A−T pair.[15,16]

The H-bonding pattern of purine nucleobases can be extended by derivatization of position 8 in the purine cycle (Figure 1). For example, 8-aminoadenine (8-NH_2A) has been shown to stabilize T·A·T triplex structures due to the formation of additional three H-bonds with thymine according to Hoogsteen-like geometry.[17−19] Its ribonucleoside 8-aminoadenosine is a potent anti-tumor agent inhibiting multiple mechanisms of transcription in mantle cell lymphoma.[20,21] The

Received: May 10, 2023
Accepted: June 21, 2023
Published: July 1, 2023

© 2023 The Authors. Published by American Chemical Society

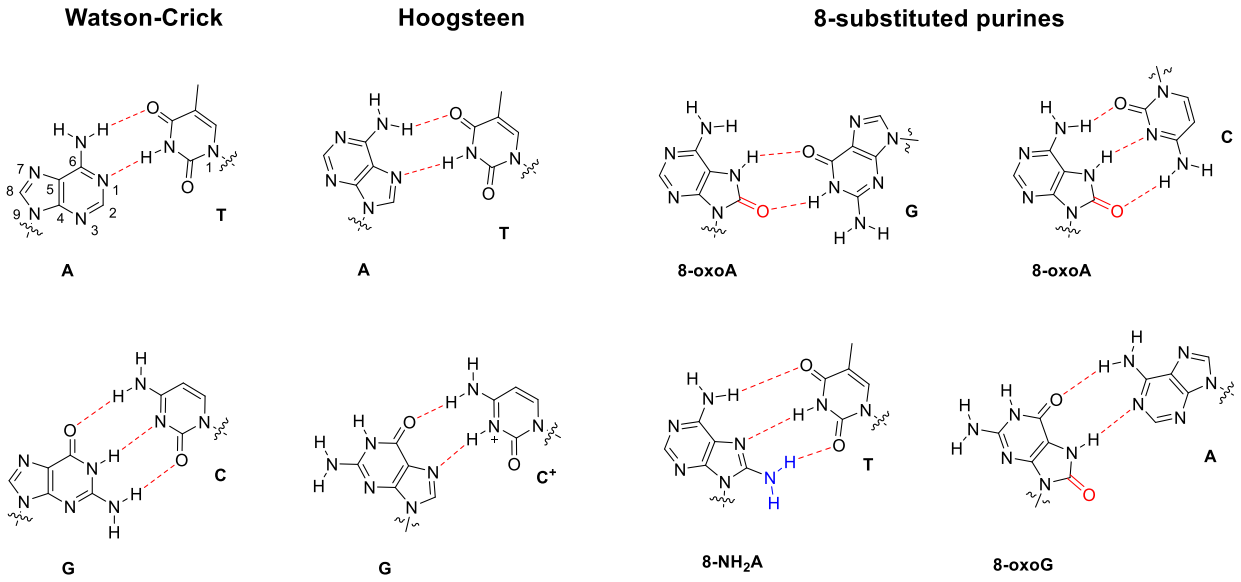

Figure 1. Bonding of nucleobases. From left to right: Watson−Crick bonding, Hoogsteen bonding, and mismatched bonding of purines substituted in position 8: 8-oxoadenine (8-oxoA), 8-aminoadenine (8-NH_2A), and 8-oxoguanine (8-oxoG).

hydrogen-bonding abilities of purines are susceptible to post-replication or post-transcription modification, such as *N*-methylation. For example, N^1- and N^6-methylated adenine derivatives tend to form Hoogsteen-like complexes with thymine.[13,22,23]

Hoogsteen base pairs have also been documented in oxidatively damaged NAs, with their formation causing base-pair mismatches and mutations.[24,25] Oxidative damage of NAs plays a crucial role in aging, mutagenesis, carcinogenesis, and the development of neurodegenerative diseases.[24,26,27] NAs are mainly oxidized by reactive oxygen species (ROS) occurring as byproducts of aerobic respiration in higher organisms.[28] ROS can be generated by ionizing radiation and can also enter the organism via environmental sources.[27,29] Many cellular components can be oxidized by ROS, with their effects on DNA understood to be most intensive over the long term.[30] Oxidation of DNA induces single- and double-strand breaks as well as damage to nucleobases.[31]

Over 20 oxidatively damaged purine and pyrimidine nucleobases are found in human DNA,[32] with 8-oxoguanine (8-oxoG, Figure 1) being the most abundant. Guanine nucleotides are major targets for ROS-mediated oxidation since the guanine heterocycle is the most electron-rich of the four bases.[30,33−35] In human cellular DNA, approximately 1 in every 100,000 guanine residues is oxidized to 8-oxoG.[24] Due to its high abundance, 8-oxoG is used as a biomarker to quantify oxidative stress levels in humans and animals.[36,37]

Oxidation of nucleobases causes a change in their H-bonding patterns and resulting bonding preferences. For example, guanine forms a canonical base pair with cytosine via three hydrogen bonds in Watson−Crick-like geometry (Figure 1), whereas 8-oxoG can also form a Hoogsteen-like base pair with adenine (Figure 1),[25,31] inducing G-to-T mutations.[38−40] Formation of the favorable 8-oxoG−A base pair is considered a major attribute in the mutagenicity of oxidized guanine lesions.[40] However, many 8-oxoG repair pathways prevent these mutations.[41,42] G-quartets are also distorted with the incorporation of an 8-oxoG residue due to incompatible H-bonding patterns in the G4 fold. Changes in the structure of G-quadruplexes may affect gene expression.[43]

Interestingly, when all guanine residues in a G-quartet are oxidized to 8-oxoG, a structurally similar 8-oxoG-quartet is formed, albeit with a larger cavity for incorporating cations.[44]

Surprisingly, another oxidized purine base and major oxidative adenine lesion—8-oxoadenine (8-oxoA, Figure 1)—has been found to be at least an order of magnitude less mutagenic in *E. coli* cells than 8-oxoG[39] and comparably mutagenic as 8-oxoG in mammalian cells.[45,46] Its cellular levels found in irradiated DNA[40] and human cancerous tissues[47] are one-third to one-half of those reported for 8-oxoG.[48,49] However, the mechanism behind 8-oxoA mutagenicity is still poorly understood. In Hoogsteen geometry, 8-oxoA prefers to form a mismatched base pair with guanine instead of a canonical base pair with thymine, which results in A-to-C mutations (Figure 1).[40]

Understanding the H-bonding abilities of modified nucleobases is a key step in uncovering the biomolecular mechanisms of mutagenesis and damaged DNA recognition. Gas-phase MS,[50] thermal denaturation of double-stranded NAs,[51] microcalorimetry,[52] and nuclear magnetic resonance (NMR) spectroscopy[53−57] have been employed in studies of H-bonding interactions between nucleobases. NMR spectroscopy is considered the most powerful tool for providing information not only on complexation energies but also on the geometries of H-bonded complexes.[13,55,57] In addition to experimental studies, bonding interactions between nucleobases have been extensively studied using computational methods.[58−65]

Here, we investigate the H-bonding interactions of 8-substituted purines, including genotoxic 8-oxoG, 8-oxoA, and the potent anti-tumor agent 8-NH_2A using NMR spectroscopy and computational chemistry. We discuss the influence of the substitution at position 8 on Watson−Crick and Hoogsteen pairings and assess whether the preference for Hoogsteen-type pairing observed previously for A and T is a general trend. We synthesized nucleobase derivatives **1**−**6** substituted with a 2-(2-(2-methoxyethoxy)ethoxy)ethyl substituent at the N9 (for **1**−**4**) and N1 (for **5**−**6**) positions (Figure 2) to increase solubility. We investigated modified nucleobases in order to get an insight into their hydrogen-bonding preferences without

https://doi.org/10.1021/acsomega.3c03244
ACS Omega 2023, 8, 25538−25548

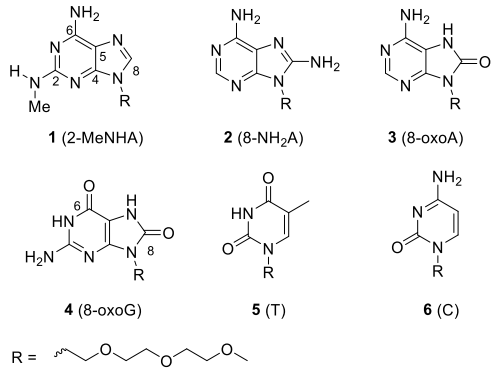

Figure 2. Structures of the studied compounds.

the bias of other factors present in NAs discussed above (e.g., backbone conformation and stacking).

RESULTS

Synthesis. Target compounds **2** and **3** were prepared from bromo derivative **8**, which was easily prepared from alcohol **7** by the Mitsunobu reaction from 8-bromoadenine[66] (Scheme 1). Compound **8** was not fully purified and used as crude. The

Scheme 1. Preparation of Compounds 2, 3, 4, and 6[a]

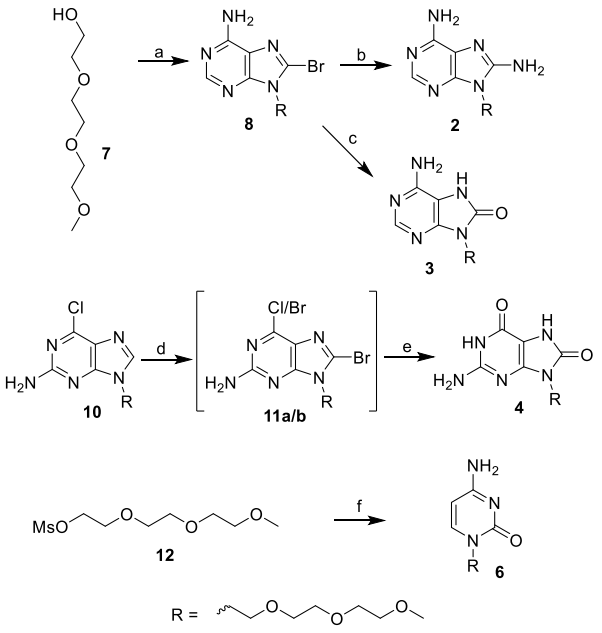

[a]Reagents and conditions: (a) 8-bromoadenine, PPh_3, DIAD, THF, 60 °C, 20 h, (b) NH_3/*i*-PrOH, dioxane, 140 °C, 7 days, (c) HCOOH, 110 °C, 2 days, (d) Br_2, H_2O−MeOH, r.t., 4 h, (e) 1. sodium acetate, acetic acid, acetic anhydride, 120 °C, 36 h, 2. aq. NH_3, methanol, 5 days, and (f) 1. N^4-acetylcytosine, Cs_2CO_3, DMF, 60 °C, 16 h, 2. NH_3/MeOH, r.t., 16 h.

bromine atom was replaced with the NH_2 group by heating of compound **8** with 2 M ammonia in isopropanol. This procedure needed a high temperature (140 °C) and prolonged time (7 days). 8-Oxo derivative **3** was prepared by heating of the bromo intermediate **8** with formic acid. Preparation of 8-oxoguanine derivative **4** started from previously described compound **10**.[53] Bromination of position 8 leads to a mixture of compounds **11a/b**. The chlorine atom in position 6 was partially replaced by bromine as confirmed by UPLC analysis of the reaction mixture. These compounds were inseparable and served as a starting material for acetolysis. 8-Oxoguanine derivative **4** was obtained after cleavage of the acetyl group by aq. ammonia. Cytosine derivative **6** was prepared from mesylate **12** (prepared according to the literature[67]) by cesium carbonate alkylation of the N^4-acetylcytosine followed by removal of the acetyl protecting group under basic conditions.

NMR Spectroscopy. In NMR spectra, the formation of intermolecular complexes can manifest in two ways. When the complex formed is stable and the complexation/decomplexation processes are slow on the NMR timescale (usually at a low temperature), two separate sets of signals can be observed—one set corresponding to free components and another set corresponding to the intermolecular complex.[53,68] When the complexation/decomplexation processes are fast on the NMR timescale, only one set of averaged signals can be observed. The chemical shift of the signals corresponds to the average shift of the free and bound species weighted according to their relative molar ratio (eq SE2 in the Supporting Information, SI). Although the observation of one or two sets of signals depends on the exchange rate between the free and bound states (i.e., controlled by kinetics), it is still closely related to the thermodynamic stabilization of the complex formed, where greater stabilization of the complex increases barriers to the decomplexation reaction.

Complexes with Two Hydrogen Bonds. Doubly bonded complexes are generally less stable than those bonded via three H-bonds.[69] In our previous work,[13] we studied complexes of methylated adenine derivatives with thymine, finding that complexation only manifested with signal shifts in NMR spectra. We also observed that the thymine molecule preferred formation of Hoogsteen-like complexes with adenine, resulting in larger signal shifts of the adenine amino hydrogen on the Hoogsteen side of the molecule.

Here, we investigate the complexation of 8-oxoA derivative **3** with thymine derivative **5**, which can form either Watson−Crick-like or Hoogsteen-like complexes, both with two hydrogen bonds. The N^7H proton and the oxygen in position 8 can pair with the thymine imido hydrogen and one of the thymine oxygen atoms in the Hoogsteen complex. We recorded a series of ^{1}H NMR spectra for 8-oxoA derivative **3** with variable molar ratios of thymine counterpart **5** in a DMF−DCM mixture (vol. 1:1) within a temperature range of 190−210 K. We observed only negligible chemical-shift changes of 8-oxoA amino protons even in the excess of the thymine derivative (Figure 3). This indicates that none of the complexes **3**−**5** (Watson−Crick- or Hoogsteen-like) was stable under these conditions.

Complexes with Three Hydrogen Bonds. Complexes with three hydrogen bonds are generally more stable than complexes with two hydrogen bonds. However, their stability depends significantly on secondary electrostatic interactions determined by the alternation of H-bonding donors (D) and acceptors (A). The association constant of ADA-type complexes (Figure 4) has been shown to be two orders of magnitude smaller than that of DDA-type complexes.[69−71] This finding is supported by the substantial electrostatic interactions between H-bond donors and acceptors bearing partial positive and negative charges, respectively. In the case of the alternating hydrogen-bonding ADA pattern (Figure 4), there are four secondary repulsive interactions. On the other hand, the DDA type (e.g., guanine−cytosine base pair) has two attractive and two repulsive secondary interactions. This

https://doi.org/10.1021/acsomega.3c03244
ACS Omega 2023, 8, 25538−25548

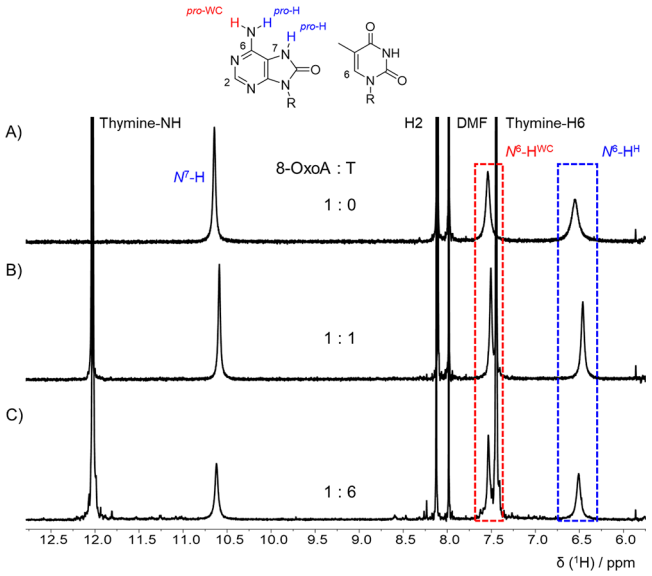

Figure 3. NH regions of ^{1}H NMR spectra of (A) 8-oxoA derivative **3** (10 mM), (B) an equimolar mixture of 8-oxoA derivative **3** (10 mM) and thymine derivative **5** (10 mM), and (C) 8-oxoA derivative **3** (10 mM) in the excess of thymine derivative **5** (60 mM) in a DMF-DCM mixture (vol. 1:1) at 190 K.

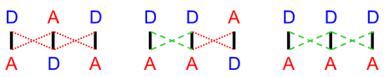

Figure 4. Types of alternations of H-bonding donors (D) and acceptors (A) in complexes with three H-bonds (black solid lines) differentiated by secondary attractive (green dashed lines) and repulsive (red dotted lines) interactions.

secondary attraction increases the stability of these H-bonded complexes (Figure 4). The greatest stability has been observed in triply bonded DDD−AAA complexes, where all four secondary interactions are attractive.[72−74]

ADA-Type Complexes. Thymine derivative **5** can form ADA-type hydrogen bonds with the Watson−Crick side of 2-(methylamino)adenine (2-MeNHA) derivative **1** and with the Hoogsteen side of 8-NH_2A derivative **2**. We analyzed chemical-shift changes of the thymine imido proton upon the addition of 8-NH_2A derivative **2** in CD_3OH in comparison with previously published results for 2-MeNHA derivative **1**.[13] We acquired a series of ^{1}H NMR spectra for samples with variable molar ratios of 8-NH_2A analogue **2** and thymine derivative **5** within a broad temperature range of 180−240 K. We observed significant chemical-shift changes in signals of hydrogen atoms involved in the intermolecular H-bond. However, we did not observe a second set of signals corresponding to the intermolecular complex, indicating a fast complexation/decomplexation rate on the NMR timescale across the whole temperature range. As depicted in Figure 5, the thymine imido proton exhibited greater chemical-shift changes upon the addition of 8-NH_2A derivative **2** than upon the excess of 2-MeNHA **1**. The increased chemical-shift changes induced by the addition of 8-NH_2A derivative **2** may be caused either by the greater stability of the Hoogsteen **2**−**5** complex or by the greater chemical shift of the proton in this complex. Note also that 2-MeNHA can have two conformations (rotamers) of the methylamino group, but only one of them (with the methyl group heading toward the nitrogen

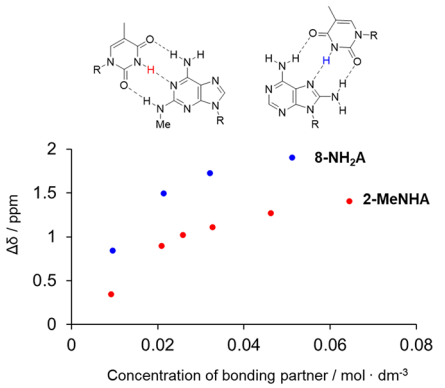

Figure 5. Chemical-shift changes of the NH imido proton of compound **5** (10 mM) in CD_3OH induced by the presence of adenine derivatives 2-MeNHA (**1**) and 8-NH_2A (**2**) at 180 K.

atom in position 3, as shown in Figure 2) can form complexes with three H-bonds.[13]

We speculated that a less polar solvent might further stabilize the intermolecular complexes. Therefore, we acquired a series of proton spectra for mixtures of 8-NH_2A derivative **2** and thymine derivative **5** in a DMF−DCM mixture (vol. 1:1) within the same temperature range of 180−240 K. In the excess of thymine derivative **5**, a new signal at an increased chemical shift of 14.5 ppm appeared at the lowest temperature of 180 K. This signal corresponded to the thymine imido proton in the H-bonded complex with compound **2** (Figure 6). No new signal was observed for the 2-MeNHA−T (**1**−**5**) system in this solvent mixture. The appearance of the imido signal in **2**−**5** thus indicates a slower complexation/decomplexation rate than in **1**−**5**. It can therefore be assumed that Hoogsteen complex **2**−**5** has greater stability. Complexation of the Hoogsteen side of 8-NH_2A was confirmed by greater chemical-shift changes of the amino protons on the Hoogsteen side of compound **2** upon the addition of thymine derivative **5** (Figure S1 in the SI).

We also studied the interactions of 2-MeNHA (**1**) and 8-NH_2A (**2**) derivatives with another ADA counterpart, 8-oxoG analogue **4**. The 8-oxoG moiety offers two bonding sites with the same H-bond count: the Watson−Crick side featuring a DDA pattern (see below) and the Hoogsteen side featuring an ADA pattern. Adenine derivatives **1** and **2** are suitable for bonding with 8-oxoG only in the Hoogsteen-like (ADA) manner. We recorded a series of ^{1}H NMR spectra of 8-oxoG derivative **4** with variable molar ratios of derivative **1** or **2** in the DMF−DCM mixture within a temperature range of 180−240 K. The addition of adenine derivatives **1** and **2** induced significant chemical-shift changes of the N^7-H proton of 8-oxoG, confirming the formation of an intermolecular complex on the Hoogsteen side of 8-oxoG. The higher chemical shift of 8-oxoG N^7-H was induced by the presence of 8-NH_2A derivative **2** (Figure S2). Similar to ADA-type complexes of thymine, a new set of signals corresponding to the intermolecular complexes **1**−**4** and **2**−**4** appeared only at the lowest temperature of 180 K.

DDA-Type Complexes. 8-OxoA derivative **3** and 8-oxoG derivative **4** are suitable complementary partners for the cytosine molecule. While 8-oxoA offers three hydrogen bonds to the AAD cytosine counterpart on the Hoogsteen side of the molecule, 8-oxoG can form three H-bonded complexes with

https://doi.org/10.1021/acsomega.3c03244
ACS Omega 2023, 8, 25538−25548

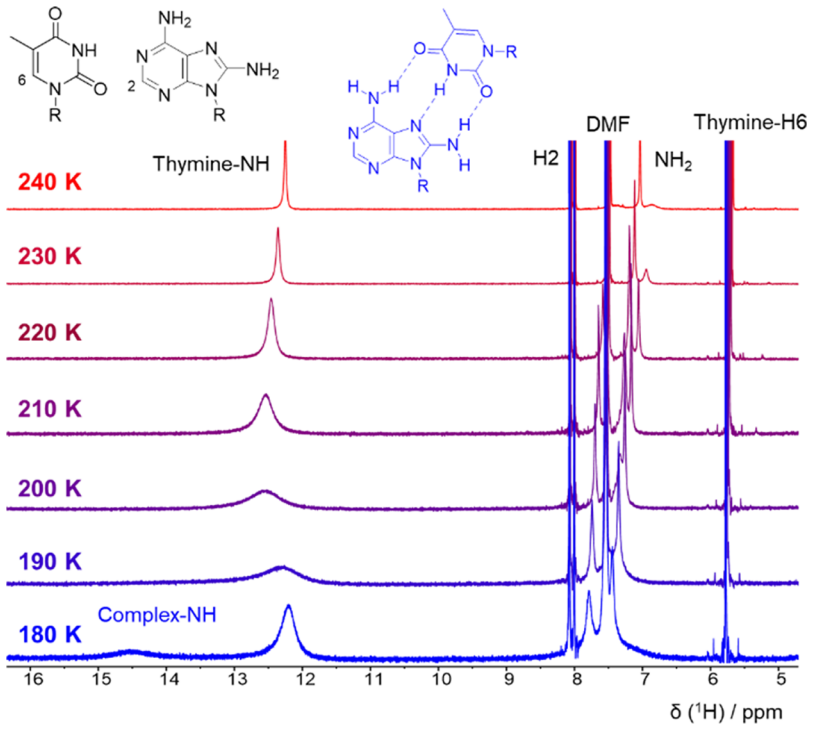

Figure 6. Aromatic and NH region of ^{1}H NMR spectra of 8-NH$_2$A derivative **2** (10 mM) in the excess of thymine derivative **5** (30 mM) in a DMF−DCM mixture (vol. 1:1) at variable temperatures.

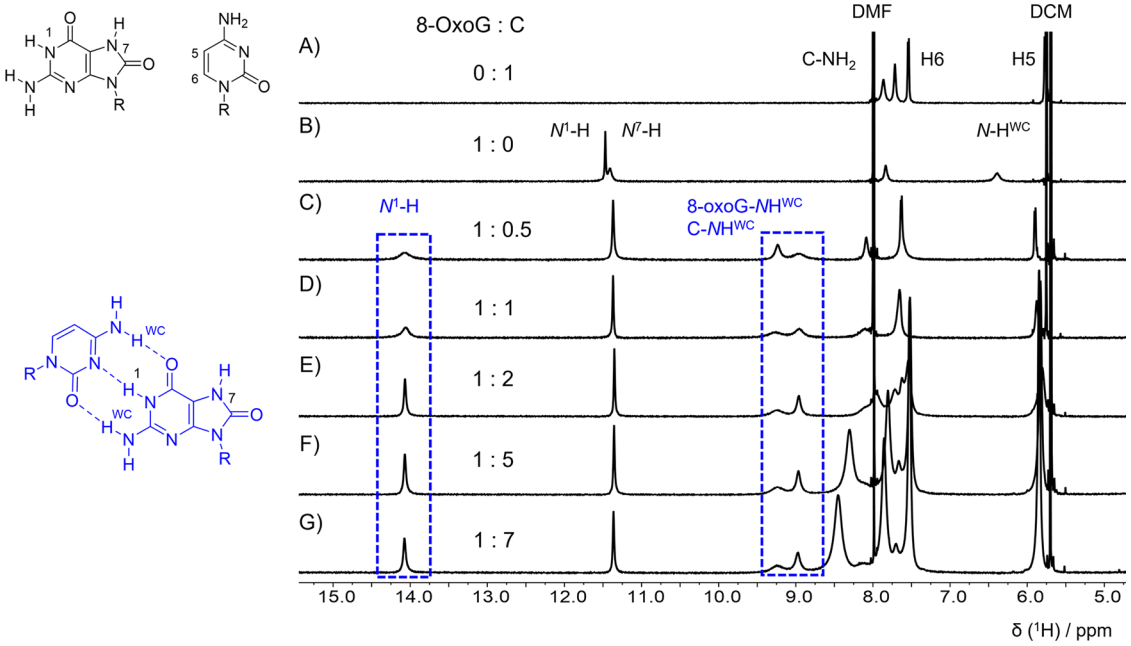

Figure 7. Aromatic and NH region of ^{1}H NMR spectra of (A) cytosine derivative **6** (10 mM), (B) 8-oxoG derivative **3** (10 mM), and (C−G) 8-oxoG derivative **3** (10 mM) with increasing concentrations of cytosine derivative **6** in a DMF−DCM mixture (vol. 1:1) at 240 K. The signals indicating **3**−**6** complex formation are highlighted in blue.

cytosine in Watson−Crick geometry (as in the canonical G−C base pair).

We investigated the intermolecular interactions of compounds **3** and **4** with cytosine derivative **6**. In contrast to the ADA-type complexes discussed above, a new set of signals corresponding to the intermolecular complex was detectable across the entire investigated temperature range of 180−240 K in the DMF−DCM solvent mixture. The chemical shift of the N^7-H signal from 8-oxoA derivative **3** in the complex was 3 ppm higher (around 14 ppm) than that of the signal of the same hydrogen atom in free compound **3** (Figure S3). We also performed a similar set of proton experiments with various mixtures of 8-oxoA and cytosine derivatives in CD$_3$OH solvent (Figure S4), with the DDA complex also formed in this solvent.

https://doi.org/10.1021/acsomega.3c03244
ACS Omega 2023, 8, 25538−25548

The Watson−Crick side of 8-oxoG derivative **4** has a similar H-bonding pattern to the Hoogsteen side of 8-oxoA. When cytosine derivative **6** was added to the solution with compound **4**, a new set of signals corresponding to the intermolecular complex appeared. The chemical shift of N^1-H in the complex was about 2.7 ppm higher (close to 14 ppm at 180 K) than that of free 8-oxoG. Furthermore, the signals of two amino protons (in position 2 of 8-oxoG and in position 4 of cytosine) involved in intermolecular H-bonding were close to 9 ppm (Figure 7).

In summary, the obtained experimental data show that the stabilization of intermolecular complexes of modified nucleobases depends on the number of H-bonds and the alternation of H-bond donors and acceptors. The complexes with two intermolecular H-bonds were not observed at all (in the case of the 8-oxoA−T system, **3**−**5**) or only served to increase the chemical shifts of amino signals (observed previously for the Hoogsteen-type A−T system). The complexes with three alternating hydrogen bonds of the ADA type were more stable than the complexes with two hydrogen bonds, which was reflected in a separate set of signals at 180 K corresponding to the intermolecular complex. The most stable complexes were those featuring three hydrogen bonds of the DDA type. The separate signals of these complexes were observed across a broad temperature range. Based on these experimental data, there was no clear difference between the stability of Watson−Crick or Hoogsteen-like complexes containing three hydrogen bonds. We did not observe any chemical-shift changes of the 2-(2-(2-methoxyethoxy)ethoxy)ethyl substituent, which confirms that this substituent does not interfere with the intermolecular H-bonding interactions.

DFT Calculations. We also performed a computational study of the 8-substituted purines and their H-bonding interactions to support the interpretation of our experimental data. We analyzed the interaction energies, geometries, and NMR parameters of the complexes. Table 1 summarizes the calculated free-energy changes of complexation of H-bonded complexes involving substituted purines **1**−**4** with their Watson−Crick and Hoogsteen partners at 200 K. Several other complexes excluded from the experimental analysis are shown in Table 1. These include the canonical G−C and A−T base pairs and the complexes with uric acid, which offer the same H-bonding pattern on both sides of the molecule (Watson−Crick and Hoogsteen). To simplify the calculations, the 2-(2-(2-methoxyethoxy)ethoxy)ethyl group was substituted with a methyl group; this simplification is justified by the absence of chemical-shift changes of the substituent upon the additions of H-bonding partners and by a conformational analysis showing that the substituent cannot participate in the Watson−Crick or Hoogsteen binding. The complexation free energies were obtained as the difference between the free energy of the complex and the sum of free energies of its components. Note that a solvent is included only implicitly in the calculations; these calculations therefore overestimate the magnitudes of the complexation energies because H-bonding interactions (and stabilization) of nucleobase monomers with solvent molecules are not covered with the implicit solvent model.[53,68]

Table 1. Calculated (B3LYP/6-311++G(2df,2pd)/PCM/GD3) Free Energies of Complexation at 200 K in DMF ($\Delta G_{complex}$, kcal/mol), Geometry of the Complexes (Watson−Crick, WC; Hoogsteen, H), and H-Bonding Alternations (HB Type)[a]

complex	geometry	H-bonds	HB type	$\Delta G_{complex}$
8-NH_2A−T (**2**−**5**)	WC	2	AD	−3.57
8-oxoA−T (**3**−**5**)	WC	2	AD	−3.14
8-oxoA−T (**3**−**5**)	H	2	AD	−3.48
A−T (**A**−**5**)	H	2	AD	−2.90
A−T (**A**−**5**)	WC	2	AD	−2.87
2-MeNHA−T (**1**−**5**)	WC	3	ADA	−5.31
8-NH_2A−T (**2**−**5**)	H	3	ADA	−6.47
8-oxoG−2-MeNHA (**4**−**1**)	H−WC	3	ADA	−5.87
8-oxoG−8NH_2A (**4**−**2**)	H−H	3	ADA	−6.74
UA−2-MeNHA (**UA**−**1**)	WC−WC	3	ADA	−5.52
UA−2-MeNHA (**UA**−**1**)	H−WC	3	ADA	−5.31
8-oxoA−C (**3**−**6**)	H	3	DDA	−8.37
8-oxoG−C (**4**−**6**)	WC	3	DDA	−8.91
G−C (**G**−**6**)	WC	3	DDA	−8.70

[a]A stands for 9-methyladenine, T for 1-methylthymine, G for 9-methylguanine, and UA for 9-methyluric acid.

In agreement with our experimental analysis, the complexation free energies are mainly controlled by the number and alternation pattern of the intermolecular H-bonds. The complexes with two H-bonds showed smaller stabilization (3−4 kcal/mol) than those connected through three H-bonds of the ADA type (5−7 kcal/mol) and DDA type (8−9 kcal/mol).

Substitution of purine nucleobases at position 8 did not lead to significant changes in the stabilization of Watson−Crick base pairs. For example, the stabilization energy of the canonical Watson−Crick A−T base pair was 2.9 kcal/mol, while stabilization energies of the Watson−Crick pairs of 8-NH_2A and 8-oxoA were 3.6 and 3.1 kcal/mol, respectively. Similarly, stabilization of the 8-oxoG−C Watson−Crick pair (8.9 kcal/mol) was only slightly higher than that of the canonical G−C pair (8.7 kcal/mol).

Stabilization energies of the Hoogsteen and Watson−Crick complexes featuring the same hydrogen-bond count and pattern were similar. For example, thymine can bind to adenine via two hydrogen bonds from both sides (Watson−Crick and Hoogsteen), and the calculated stabilization energies are almost identical (2.9 kcal/mol) for both complexes. In the case of thymine bound via three hydrogen bonds of the ADA type to the Watson−Crick side of 2-MeNHA and to the Hoogsteen side of 8-NH_2A, stabilization of the latter complex (6.5 kcal/mol) was slightly higher than that of the former (5.3 kcal/mol). Finally, in the case of cytosine bound via three DDA-type H-bonds to the Watson−Crick side of guanine and 8-oxoG as well as to the Hoogsteen side of 8-oxoA, stabilization energies were similar for all three complexes (8.4−8.9 kcal/mol).

Geometries of the intermolecular H-bonds in both Watson−Crick and Hoogsteen complexes were close to optimal for strong binding. All distances between the hydrogen atom from the donor group and the acceptor atom fell within a range of 1.80−1.94 Å, while the O−H···N and N−H···N angles were close to the ideal value of 180° (see Table S1 in the SI).

We also calculated chemical-shift changes of hydrogen atoms induced by the formation of intermolecular complexes. Unsurprisingly, the greatest changes were observed for hydrogen atoms involved in H-bonding (Table S2). These calculations retrospectively confirmed the assignment of signals in the experimental spectra. For example, imido protons (N^1-H

https://doi.org/10.1021/acsomega.3c03244
ACS Omega 2023, 8, 25538−25548

in G, N^7-H in 8-oxoG and 8-oxoA, and N^3-H in T) in complexes were less shielded (having higher chemical shifts) than amino protons participating in H-bonding. Experimental spectra demonstrated greater chemical-shift changes of the thymine imido proton upon formation of the Hoogsteen complex with 8-NH_2A than upon formation of the Watson−Crick complex with 2-MeNHA (Figure 5). These observations correlate with our calculations, which predicted a 0.65 ppm higher chemical shift for the imido proton in the 8-NH_2A−T complex than in the 2-MeNHA−T complex. This may have been due to the shorter interatomic distance between the thymine imido proton and N^7 of the purine ring than that between thymine and nitrogen N^1 in Watson−Crick-like complex **1**−**5**. Similarly, chemical-shift changes of N^7-H in 8-oxoG were greater in the ADA-type Hoogsteen complex with 8-NH_2A than those in the Watson−Crick complex with 2-MeNHA (about 0.58 ppm), which corresponds with our experimental analysis.

METHODS

Synthesis. Thymine derivative **5** and 2-MeNHA derivative **1** were synthesized using protocols published previously.[13,68]

NMR spectra (δ, ppm; J, Hz) were measured on a Bruker Avance III HD 500 MHz instrument equipped with a cryoprobe (500.0 MHz for ^{1}H and 126 MHz for ^{13}C) in hexadeuterated dimethyl sulfoxide and referenced to the solvent signal (δ 2.50 and 39.70). Mass spectra were measured on an LTQ Orbitrap XL (Thermo Fisher Scientific) using electrospray ionization. Column chromatography was performed on silica gel 60 (Fluka) and thin-layer chromatography on silica gel 60 F254 foils (Merck). Solvents were evaporated at 2 kPa and bath temperatures of 30−60 °C; the compounds were dried at 13 Pa and 50 °C. UPLC samples were measured on the Waters UPLC H-Class Core System (column Waters Acquity UPLC BEH C18 1.7 μm, 2.1 × 100 mm), Waters Acquity UPLC PDA detector, mass spectrometer Waters SQD2, and MassLynx Mass Spectrometry Software. For reverse-phase flash column chromatography, C-18 RediSep Rf column Teledyne ISCO was used.

*8-Bromo-9-(2-(2-(2-methoxyethoxy)ethoxy)ethyl)-9H-purin-6-amine (**8**).* A suspension of 8-bromoadenine (1.261 g, 5.9 mmol), triphenylphosphine (2.02 g, 7.68 mmol), and alcohol **7** (1.23 mL, 6.3 mmol) in THF (30 mL) was heated to 60 °C (bath). DIAD (1.51 mL, 7.7 mmol) was dropwise added to this reaction mixture during 10 min. Heating continued for 18 h, and then, the second portion of the reagents was added [PPh_3 (2.02 g, 7.68 mmol); alcohol **7** (1.23 mL, 6.3 mmol); DIAD (1.51 mL, 7.7 mmol)]. The reaction mixture was heated for another 2 h, cooled down, evaporated, and the crude residue was purified by reverse-phase chromatography (320 g column, water−acetonitrile 10% → 50%). Fractions containing the product were evaporated (1.49 g) and used in the next step. UPLC-MS: t = 2.72 (M + H, 360.2/362.2).

*9-(2-(2-(2-Methoxyethoxy)ethoxy)ethyl)-9H-purine-6,8-diamine (**2**).* Crude compound **8** (271 mg, 0.75 mmol) was dissolved in dioxane (5 mL) and NH_3/*i*-PrOH (2 M, 20 mL) in a pressure flask. The reaction mixture was heated to 140 °C for 7 days. Fresh NH_3/*i*-PrOH (2 M, 10 mL) was added every second day to the flask. The reaction mixture was cooled down, evaporated, and the product was isolated by reverse-phase chromatography (220 g column, water−acetonitrile 0% → 30%). 118 mg (53%) of the product was obtained as a white foam after lyophilization from dioxane. HRMS calcd for $C_{12}H_{21}N_6O_3$ m/z: 297.16697 $(M + H)^+$, found 297.16701. ^{1}H NMR (500 MHz, d_6-DMSO): δ = 7.89 (s, 1H, H2), 6.35 (bs, 2H, C6-NH_2), 6.32 (bs, 2H, C8-NH_2), 4.10 (t, 2H, ^3J = 5.8 Hz, H1′), 3.68 (t, 2H, ^3J = 5.8 Hz, H2′), 3.55−3.50 (m, 2H, H3′), 3.48−3.42 (m, 4H, H4′, H5′), 3.41−3.35 (m, 2H, H6′), 3.21 (s, 3H, H7′) ppm. ^{13}C{^{1}H} NMR (126 MHz, d_6-DMSO): δ = 152.2 (C8), 152.0 (C6), 149.9 (C4), 148.6 (C2), 116.9 (C5), 71.2 (C6′), 69.7, 69.6 (3C, C3′, C4′, and C5′), 68.1 (C2′), 58.0 (C7′), 40.4 (C1′) ppm.

*6-Amino-9-(2-(2-(2-methoxyethoxy)ethoxy)ethyl)-7,9-dihydro-8H-purin-8-one (**3**).* Crude compound **8** (354 mg, 0.98 mmol) was heated in formic acid (concentrated, 20 mL) at 110 °C (bath) for 2 days. Then, volatiles were evaporated, and the residue was co-evaporated with ethanol (2 × 50 mL). The residue was re-dissolved in ethanol (25 mL) and aq. ammonia (5 mL) and stirred at r.t. for 15 min and evaporated. The product was isolated by reverse-phase chromatography (220 g column, water−acetonitrile 0% → 20%). 163 mg (56%) of the product was obtained as a white foam after lyophilization from dioxane. HRMS calcd for $C_{12}H_{19}N_5O_4Na$ m/z: 320.13293 $(M + Na)^+$, found 320.13298. ^{1}H NMR (500 MHz, d_6-DMSO): δ = 10.34 (bs, 1H, N^7-H), 8.00 (s, 1H, H2), 6.46 (bs, 2H, NH_2), 3.88 (t, 2H, ^3J = 6.0 Hz, H1′), 3.69 (t, 2H, ^3J = 6.0 Hz, H2′), 3.52−3.48 (m, 2H, H3′), 3.46−3.40 (m, 4H, H4′, H5′), 3.38−3.34 (m, 2H, H6′), 3.20 (s, 3H, H7′) ppm. ^{13}C{^{1}H} NMR (126 MHz, d_6-DMSO): δ = 152.4 (C8), 150.8 (C2), 147.7 (C4), 146.7 (C6), 103.6 (C5), 71.2 (C6′), 69.6, 69.4 (C3′, C4′, and C5′), 66.9 (C2′), 58.0 (C7′), 38.8 (C1′) ppm.

*2-Amino-9-(2-(2-(2-methoxyethoxy)ethoxy)ethyl)-7,9-dihydro-1H-purine-6,8-dione (**4**).* Compound **10** (1.206 g, 3.8 mmol) was dissolved in a water−methanol mixture (2:1, 90 mL), and bromine (0.25 mL, 4.9 mmol) was added at r.t. The reaction mixture was stirred for 4 h and then evaporated. Intermediate **11** was isolated as a mixture of chloro and bromo derivatives in position 6 by reverse-phase chromatography (220 g column, water−methanol 10% → 90%). Fractions containing the product were evaporated. The residue was co-evaporated with ethanol (3 × 50 mL) and dioxane (50 mL). The obtained residue was used immediately in the next step. Sodium acetate (1.6 g), acetic anhydride (7.5 mL), and acetic acid (46 mL) were added, and the reaction mixture was heated to 120 °C for 36 h. The reaction mixture was then cooled down, evaporated, and re-dissolved in methanol (25 mL) and aq. ammonia (25 mL) and stirred at r.t. for another 5 days. The product was isolated by reverse-phase chromatography (220 g column, water−acetonitrile 0% → 30%). 393 mg (33%) of the product was obtained as a white foam after lyophilization from dioxane. HRMS calcd for $C_{12}H_{19}N_5O_5Na$ m/z: 336.12784 $(M + Na)^+$, found 336.12790. ^{1}H NMR (500 MHz, d_6-DMSO): δ = 10.66 (bs, 1H, N^1-H), 10.52 (bs, 1H, N^7-H), 6.49 (bs, 2H, NH_2), 3.74 (t, 2H, ^3J = 6.2 Hz, H1′), 3.61 (t, 2H, ^3J = 6.2 Hz, H2′), 3.54−3.48 (m, 2H, H3′, H4′, or H5′), 3.48−3.42 (m, 4H, H3′, H4′, or H5′), 3.41−3.36 (m, 2H, H6′), 3.22 (s, 3H, H7′) ppm. ^{13}C{^{1}H} NMR (126 MHz, d_6-DMSO): δ = 153.5 (C2 or C6), 152.3 (C8), 151.0 (C2 or C6), 148.1 (C4), 98.2 (C5), 71.3 (C6′), 69.6 (3C, C3′, C4′, and C5′), 67.1 (C2′), 58.0 (C7′), 38.6 (C1′) ppm.

*4-Amino-1-(2-(2-(2-methoxyethoxy)ethoxy)ethyl)-pyrimidin-2(1H)-one (**6**).* N^4-Acetylcytosine (1.865 g, 12.2 mmol) was dissolved in a solution of mesylate **12** (1.47 g, 6.1 mmol) in DMF (30 mL), and to this mixture was added Cs_2CO_3 (2.99 g, 9.1 mmol) at r.t. The reaction mixture was then heated to 60 °C (bath) for 16 h, cooled down, and

https://doi.org/10.1021/acsomega.3c03244
ACS Omega 2023, 8, 25538−25548

evaporated. Solids were extracted with portions of an acetone−ethyl acetate mixture. The solution was evaporated and the residue was chromatographed on a reverse-phase column (220 g column, water−acetonitrile 5% → 50%). Fractions containing the intermediate were evaporated and then dissolved in NH_3/MeOH (10 M, 30 mL). The reaction mixture was stirred at r.t. for 16 h and then evaporated. The product was isolated by reverse-phase chromatography (220 g column, water−acetonitrile 0% → 20%). After lyophilization (dioxane), 863 mg (55%) of product **6** was obtained. HRMS calcd for $C_{11}H_{19}N_3O_4Na$ m/z: 280.12678 $(M + Na)^+$, found 280.12653. ^{1}H NMR (500 MHz, d_6-DMSO): δ = 7.49 (d, 1H, ^3J = 7.1 Hz, H4), 7.01 (bs, 1H, NH_2), 6.91 (bs, 1H, NH_2), 5.59 (d, 1H, ^3J = 7.1 Hz, H5), 3.77 (t, 2H, ^3J = 5.3 Hz, H1′), 3.56 (t, 2H, ^3J = 5.3 Hz, H2′), 3.51−3.44 (m, 6H, H3′, H4′, H5′), 3.43−3.38 (m, 2H, H6′), 3.23 (s, 3H, H7′) ppm. ^{13}C{^{1}H} NMR (126 MHz, d_6-DMSO): δ = 166.0 (C6), 155.7 (C2), 146.8 (C4), 92.7 (C5), 71.3 (C6′), 69.7, 69.6 (3C, C3′, C4′, and C5′), 58.1 (C7′), 68.2 (C2′), 48.3 (C1′) ppm.

NMR Experiments. ^{1}H and ^{13}C NMR spectra were recorded on a 500 MHz NMR spectrometer (^{1}H at 500 MHz and ^{13}C at 126 MHz) in a DMF-d_7/DCM-d_2 mixture (vol. 1:1) and CD_3OH. These solvents were selected because they allow measurements at very low temperatures. Spectra were referenced to the solvent signal δ = 2.75 and δ = 3.31, respectively. Characterization spectra of the newly prepared compounds were recorded on a 500 MHz NMR spectrometer (^{1}H at 500 MHz and ^{13}C at 126 MHz) in DMSO-d_6 [δ = 2.50 (^{1}H) and δ = 39.70 (^{13}C)]. Complete signal assignment was based on the homo- and hetero-nuclear correlation experiments COSY, HSQC, and HMBC. Solvents used in the experiments were purchased from Eurisotop (DMF-d_7, DCM-d_2, and CD_3OH in 750 μL ampoules).

Computations. The analyzed structures were refined using geometry optimization at the density functional theory (DFT) level using the B3LYP functional[75,76] with a standard 6-311++G(2df,2pd) basis set. The polarizable continuum model was used for implicit DMF and methanol solvation.[77,78] Empirical dispersion correction (GD3) was used for all calculations.[79] For the purpose of simplification, the R alkyl chain (see Figure 2) in each compound was replaced by a methyl group. Vibrational frequencies and free energies were calculated for all optimized structures to confirm the character of the minimum stationary point. Gaussian 16 software was used throughout the study.[80] No corrections of basis set superposition error (BSSE) were included in the computations of intermolecular complexes. This was based on the assumption that the large basis set used in the calculations would minimize this error.

CONCLUSIONS

We performed a combined experimental and computational study of H-bonding interactions of nucleobases substituted in position 8. Our experimental findings are based on changes in ^{1}H NMR spectra induced by the addition of suitable H-bonding partners. DFT-derived computations produced free energies of complexation, complex geometries, and chemical shielding.

Both our experiments and computations show that stabilization of H-bonded complexes between nucleobases depends on the number of H-bonds and the alternation of H-bond donors and acceptors. Intermolecular complexes with two H-bonds exhibited relatively low stability and mostly dissociated into their individual components (nucleobases) even at 180 K.

Complexes with three intermolecular H-bonding interactions formed two clearly distinguishable groups based on differences in the alternation of H-bond donors and acceptors. Complexes of the ADA type were stable enough to generate a separate set of NMR signals at 180 K. Complexation/decomplexation processes at higher temperatures resulted in averaged NMR signals of complexes and their individual components. On the other hand, complexes with three H-bonds of the DDA type generated well-distinguished separate NMR signals across a broad temperature range. Our observation of separate signals of these complexes confirmed their greater stability, leading to higher barriers and slower rates of decomplexation.

Our computations confirmed the lowest stability of complexes with two H-bonds (stabilization of 2.9−3.6 kcal/mol) followed by complexes with three H-bonds of the ADA type (5.3−6.7 kcal/mol) and complexes of the DDA type (8.4−8.9 kcal/mol). Bonding geometry (Watson−Crick or Hoogsteen) was not a substantial contributory factor in the stability of the complexes.

In summary, this combined experimental and computational analysis demonstrated no clear differences in the stability of Watson−Crick and Hoogsteen-like nucleobase complexes. Stabilization was mostly influenced by the number and D−A alternation of intermolecular H-bonds. The preference for Watson−Crick pairing in DNA is thus mostly controlled by the conformation of the backbone. Moreover, the stabilizing effect of Hoogsteen binding in non-canonical NA structures and complexes seems to be similar to that of Watson−Crick pairing.

ASSOCIATED CONTENT

Supporting Information

The Supporting Information is available free of charge at https://pubs.acs.org/doi/10.1021/acsomega.3c03244.

Additional NMR spectra, NMR and HRMS spectra of the prepared compounds, calculated free energies of complexation, calculated chemical-shift changes upon complexation, and Cartesian coordinates (PDF)

AUTHOR INFORMATION

Corresponding Author

Martin Dračínský − *Institute of Organic Chemistry and Biochemistry of the Czech Academy of Sciences, 160 00 Prague 6, Czech Republic;* orcid.org/0000-0002-4495-0070; Email: dracinsky@uochb.cas.cz

Authors

Zuzana Osifová − *Institute of Organic Chemistry and Biochemistry of the Czech Academy of Sciences, 160 00 Prague 6, Czech Republic; Department of Organic Chemistry, Faculty of Science, Charles University, 128 00 Prague, Czech Republic*

Michal Šála − *Institute of Organic Chemistry and Biochemistry of the Czech Academy of Sciences, 160 00 Prague 6, Czech Republic*

Complete contact information is available at: https://pubs.acs.org/10.1021/acsomega.3c03244

https://doi.org/10.1021/acsomega.3c03244
ACS Omega 2023, 8, 25538−25548

Notes

The authors declare no competing financial interest.

■ ACKNOWLEDGMENTS

This work was supported by the Charles University Grant Agency (grant no. 302922) and the Czech Science Foundation (grant no. 22-15374S). We wish to thank Dr. Lucie Mužíková-Čechová for the preparation of compound **1**.

■ REFERENCES

(1) Watson, J. D.; Crick, F. H. C. Genetical Implications of the Structure of Deoxyribonucleic Acid. *Nature* **1953**, *171*, 964−967.
(2) Hoogsteen, K. The Structure of Crystals Containing a Hydrogen-Bonded Complex of 1-Methylthymine and 9-Methyladenine. *Acta Crystallogr.* **1959**, *12*, 822−823.
(3) Abrescia, N. G. A.; Thompson, A.; Huynh-Dinh, T.; Subirana, J. A. Crystal structure of an antiparallel DNA fragment with Hoogsteen base pairing. *Proc. Natl. Acad. Sci. U. S. A.* **2002**, *99*, 2806−2811.
(4) Sklenář, V.; Feigon, J. Formation of a Stable Triplex from a Single DNA Strand. *Nature* **1990**, *345*, 836−838.
(5) Lipps, H. J.; Rhodes, D. G-quadruplex structures: in vivo evidence and function. *Trends Cell. Biol.* **2009**, *19*, 414−422.
(6) Balasubramanian, S.; Neidle, S. G-quadruplex nucleic acids as therapeutic targets. *Curr. Opin. Chem. Biol.* **2009**, *13*, 345−353.
(7) Varshney, D.; Spiegel, J.; Zyner, K.; Tannahill, D.; Balasubramanian, S. The regulation and functions of DNA and RNA G-quadruplexes. *Nat. Rev. Mol. Cell Biol.* **2020**, *21*, 459−474.
(8) Rice, P. A.; Yang, S. W.; Mizuuchi, K.; Nash, H. A. Crystal structure of an IHF-DNA complex: A protein-induced DNA U-turn. *Cell* **1996**, *87*, 1295−1306.
(9) Wang, A. H. J.; Ughetto, G.; Quigley, G. J.; Hakoshima, T.; Vandermarel, G. A.; Vanboom, J. H.; Rich, A. The Molecular-Structure of a DNA Triostin-a Complex. *Science* **1984**, *225*, 1115−1121.
(10) Takahashi, S.; Sugimoto, N. Watson-Crick versus Hoogsteen Base Pairs: Chemical Strategy to Encode and Express Genetic Information in Life. *Acc. Chem. Res.* **2021**, *54*, 2110−2120.
(11) Sen, D.; Gilbert, W. A Sodium-Potassium Switch in the Formation of 4-Stranded G4-DNA. *Nature* **1990**, *344*, 410−414.
(12) Sen, D.; Gilbert, W. Formation of Parallel 4-Stranded Complexes by Guanine-Rich Motifs in DNA and Its Implications for Meiosis. *Nature* **1988**, *334*, 364−366.
(13) Osifová, Z.; Socha, O.; Mužíková-Čechova, L.; Šála, M.; Janeba, Z.; Dračínský, M. Hydrogen-Bonding Interactions of Methylated Adenine Derivatives. *Eur. J. Org. Chem.* **2021**, *2021*, 4166−4173.
(14) Kyogoku, Y.; Higuchi, S.; Tsuboi, M. Infra-Red Absorption Spectra of Single Crystals of 1-Methyl-Thymine 9-Methyladenine and Their 1:1complex. *Spectrochim. Acta, Part A* **1967**, *A 23*, 969−983.
(15) Kyogoku, Y.; Lord, R. C.; Rich, A. Hydrogen Bonding Specificity of Nucleic Acid Purines and Pyrimidines in Solution. *Science* **1966**, *154*, 518−520.
(16) Kyogoku, Y.; Lord, R. C.; Rich, A. An Infrared Study of Hydrogen-Bonding Specificity of Hypoxanthine and Other Nucleic Acid Derivatives. *Biochim. Biophys. Acta* **1969**, *179*, 10−17.
(17) Kawai, K.; Saito, I.; Sugiyama, H. Stabilization of Hoogsteen base pairing by introduction of NH_2 group at the C8 position of adenine. *Tetrahedron Lett.* **1998**, *39*, 5221−5224.
(18) Ganesh, K. N.; Gourishankar, A.; Vysabhattar, R.; Bokil, P. Property editing of peptide nucleic acids (PNA): gem-dimethyl, cyanuryl and 8-aminoadenine PNAs. *Nucleic Acids Symp. Ser.* **2007**, 17−18.
(19) Pezo, V.; Jaziri, F.; Bourguignon, P. Y.; Louis, D.; Jacobs-Sera, D.; Rozenski, J.; Pochet, S.; Herdewijn, P.; Hatfull, G. F.; Kaminski, P. A.; Marliere, P. Noncanonical DNA polymerization by aminoadenine-based siphoviruses. *Science* **2021**, *372*, 520−524.
(20) Dennison, J. B.; Shanmugam, M.; Ayres, M. L.; Qian, J.; Krett, N. L.; Medeiros, L. J.; Neelapu, S. S.; Rosen, S. T.; Gandhi, V. 8-Aminoadenosine inhibits Akt/mTOR and Erk signaling in mantle cell lymphoma. *Blood* **2010**, *116*, 5622−5630.
(21) Frey, J. A.; Gandhi, V. 8-Amino-Adenosine Inhibits Multiple Mechanisms of Transcription. *Mol. Cancer Ther.* **2010**, *9*, 236−245.
(22) Yang, H.; Zhan, Y. Q.; Fenn, D.; Chi, L. M.; Lam, S. L. Effect of 1-methyladenine on double-helical DNA structures. *FEBS Lett.* **2008**, *582*, 1629−1633.
(23) Lu, L. H.; Yi, C. Q.; Jian, X.; Zheng, G. Q.; He, C. A. Structure determination of DNA methylation lesions N^1-meA and N^3-meC in duplex DNA using a cross-linked protein-DNA system. *Nucleic Acids Res.* **2010**, *38*, 4415−4425.
(24) Grollman, A. P.; Moriya, M. Mutagenesis by 8-Oxoguanine - an Enemy Within. *Trends Genet.* **1993**, *9*, 246−249.
(25) Bruner, S. D.; Norman, D. P. G.; Verdine, G. L. Structural basis for recognition and repair of the endogenous mutagen 8-oxoguanine in DNA. *Nature* **2000**, *403*, 859−866.
(26) Alam, Z. I.; Jenner, A.; Daniel, S. E.; Lees, A. J.; Cairns, N.; Marsden, C. D.; Jenner, P.; Halliwell, B. Oxidative DNA damage in the parkinsonian brain: An apparent selective increase in 8-hydroxyguanine levels in substantia nigra. *J. Neurochem.* **1997**, *69*, 1196−1203.
(27) Breimer, L. H. Molecular Mechanisms of Oxygen Radical Carcinogenesis and Mutagenesis - the Role of DNA-Base Damage. *Mol. Carcinog.* **1990**, *3*, 188−197.
(28) Sabharwal, S. S.; Schumacker, P. T. Mitochondrial ROS in cancer: initiators, amplifiers or an Achilles' heel? *Nat. Rev. Cancer* **2014**, *14*, 709−721.
(29) Frenkel, K. Carcinogen-Mediated Oxidant Formation and Oxidative DNA Damage. *Pharmacol. Therapeut.* **1992**, *53*, 127−166.
(30) Fleming, A. M.; Burrows, C. J. Formation and processing of DNA damage substrates for the hNEIL enzymes. *Free Radical Biol. Med.* **2017**, *107*, 35−52.
(31) De Bont, R.; van Larebeke, N. Endogenous DNA damage in humans: a review of quantitative data. *Mutagenesis* **2004**, *19*, 169−185.
(32) Gajewski, E.; Rao, G.; Nackerdien, Z.; Dizdaroglu, M. Modification of DNA Bases in Mammalian Chromatin by Radiation-Generated Free-Radicals. *Biochemistry* **1990**, *29*, 7876−7882.
(33) Steenken, S.; Jovanovic, S. V. How easily oxidizable is DNA? One-electron reduction potentials of adenosine and guanosine radicals in aqueous solution. *J. Am. Chem. Soc.* **1997**, *119*, 617−618.
(34) Fleming, A. M.; Burrows, C. J. Interplay of Guanine Oxidation and G-Quadruplex Folding in Gene Promoters. *J. Am. Chem. Soc.* **2020**, *142*, 1115−1136.
(35) Liska, A.; Triskova, I.; Ludvik, J.; Trnkova, L. Oxidation potentials of guanine, guanosine and guanosine-5′-monophosphate: Theory and experiment. *Electrochim. Acta* **2019**, *318*, 108−119.
(36) Cathcart, R.; Schwiers, E.; Saul, R. L.; Ames, B. N. Thymine Glycol and Thymidine Glycol in Human and Rat Urine - a Possible Assay for Oxidative DNA Damage. *Proc. Natl. Acad. Sci. U. S. A.* **1984**, *81*, 5633−5637.
(37) Shigenaga, M. K.; Gimeno, C. J.; Ames, B. N. Urinary 8-Hydroxy-2'-Deoxyguanosine as a Biological Marker of Invivo Oxidative DNA Damage. *Proc. Natl. Acad. Sci. U. S. A.* **1989**, *86*, 9697−9701.
(38) Mangerich, A.; Knutson, C. G.; Parry, N. M.; Muthupalani, S.; Ye, W. J.; Prestwich, E.; Cui, L.; McFaline, J. L.; Mobley, M.; Ge, Z. M.; Taghizadeh, K.; Wishnok, J. S.; Wogan, G. N.; Fox, J. G.; Tannenbaum, S. R.; Dedon, P. C. Infection-induced colitis in mice causes dynamic and tissue-specific changes in stress response and DNA damage leading to colon cancer. *Proc. Natl. Acad. Sci. U. S. A.* **2012**, *109*, E1820−E1829.
(39) Wood, M. L.; Esteve, A.; Morningstar, M. L.; Kuziemko, G. M.; Essigmann, J. M. Genetic-Effects of Oxidative DNA Damage - Comparative Mutagenesis of 7,8-Dihydro-8-Oxoguanine and 7,8-Dihydro-8-Oxoadenine in Escherichia-Coli. *Nucleic Acids Res.* **1992**, *20*, 6023−6032.

https://doi.org/10.1021/acsomega.3c03244
ACS Omega 2023, 8, 25538−25548

(40) Koag, M. C.; Jung, H. M.; Lee, S. Mutagenesis mechanism of the major oxidative adenine lesion 7,8-dihydro-8-oxoadenine. *Nucleic Acids Res.* **2020**, *48*, 5119−5134.
(41) Raetz, A. G.; David, S. S. When you're strange: Unusual features of the MUTYH glycosylase and implications in cancer. *DNA Repair* **2019**, *80*, 16−25.
(42) Out, A. A.; Tops, C. M. J.; Nielsen, M.; Weiss, M. M.; van Minderhout, I. J. H. M.; Fokkema, I. F. A. C.; Buisine, M. P.; Claes, K.; Colas, C.; Fodde, R.; Fostira, F.; Franken, P. F.; Gaustadnes, M.; Heinimann, K.; Hodgson, S. V.; Hogervorst, F. B. L.; Holinski-Feder, E.; Lagerstedt-Robinson, K.; Olschwang, S.; van den Ouweland, A. M. W.; Redeker, E. J. W.; Scott, R. J.; Vankeirsbilck, B.; Gronlund, R. V.; Wijnen, J. T.; Wikman, F. P.; Aretz, S.; Sampson, J. R.; Devilee, P.; den Dunnen, J. T.; Hes, F. J. Leiden Open Variation Database of the MUTYH Gene. *Hum. Mutat.* **2010**, *31*, 1205−1215.
(43) Fleming, A. M.; Zhu, J.; Manage, S. A. H.; Burrows, C. J. Human NEIL3 Gene Expression Regulated by Epigenetic-Like Oxidative DNA Modification. *J. Am. Chem. Soc.* **2019**, *141*, 11036−11049.
(44) Aleksič, S.; Podbevšek, P.; Plavec, J. 8-Oxoguanine Forms Quartets with a Large Central Cavity. *Biochemistry* **2022**, *2022*, 2390−2397.
(45) Kamiya, H.; Miura, H.; Muratakamiya, N.; Ishikawa, H.; Sakaguchi, T.; Inoue, H.; Sasaki, T.; Masutani, C.; Hanaoka, F.; Nishimura, S.; Ohtsuka, E. 8-Hydroxyadenine (7,8-Dihydro-8-Oxoadenine) Induces Misincorporation in *in vitro* DNA-Synthesis and Mutations in NIH 3T3 Cells. *Nucleic Acids Res.* **1995**, *23*, 2893−2899.
(46) Tan, X. Z.; Grollman, A. P.; Shibutani, S. Comparison of the mutagenic properties of 8-oxo-7,8-dihydro-2′-deoxyadenosine and 8-oxo-7,8-dihydro-2′-deoxyguanosine DNA lesions in mammalian cells. *Carcinogenesis* **1999**, *20*, 2287−2292.
(47) Olinski, R.; Zastawny, T.; Budzbon, J.; Skokowski, J.; Zegarski, W.; Dizdaroglu, M. DNA-Base Modifications in Chromatin of Human Cancerous Tissues. *FEBS Lett.* **1992**, *309*, 193−198.
(48) Jaruga, P.; Dizdaroglu, M. Repair of products of oxidative DNA base damage in human cells. *Nucleic Acids Res.* **1996**, *24*, 1389−1394.
(49) Fuciarelli, A. F.; Wegher, B. J.; Gajewski, E.; Dizdaroglu, M.; Blakely, W. F. Quantitative Measurement of Radiation-Induced Base Products in DNA Using Gas-Chromatography Mass-Spectrometry. *Radiat. Res.* **1989**, *119*, 219−231.
(50) Dey, M.; Moritz, F.; Grotemeyer, J.; Schlag, E. W. Base-Pair Formation of Free Nucleobases and Mononucleosides in the Gas-Phase. *J. Am. Chem. Soc.* **1994**, *116*, 9211−9215.
(51) Vologodskii, A.; Frank-Kamenetskii, M. D. Theoretical model, its parameters and predictions Reply to comments on "DNA melting and energetics of the double helix". *Phys. Life Rev.* **2018**, *25*, 42−44.
(52) Hughesman, C. B.; Turner, R. F. B.; Haynes, C. A. Role of the Heat Capacity Change in Understanding and Modeling Melting Thermodynamics of Complementary Duplexes Containing Standard and Nucleobase-Modified LNA. *Biochemistry* **2011**, *50*, 5354−5368.
(53) Pohl, R.; Socha, O.; Šála, M.; Rejman, D.; Dračínský, M. The Control of the Tautomeric Equilibrium of Isocytosine by Intermolecular Interactions. *Eur. J. Org. Chem.* **2018**, *2018*, 5128−5135.
(54) Schlund, S.; Mladenovic, M.; Janke, E. M. B.; Engels, B.; Weisz, K. Geometry and cooperativity effects in adenosine-carboxylic acid complexes. *J. Am. Chem. Soc.* **2005**, *127*, 16151−16158.
(55) Dunger, A.; Limbach, H. H.; Weisz, K. Geometry and strength of hydrogen bonds in complexes of 2′-deoxyadenosine with 2′-deoxyuridine. *J. Am. Chem. Soc.* **2000**, *122*, 10109−10114.
(56) Janke, E. M. B.; Dunger, A.; Limbach, H. H.; Weisz, K. Hydrogen bonding in complexes of adenosine and 4-thiouridine: a low-temperature NMR study. *Magn. Reson. Chem.* **2001**, *39*, S177−S182.
(57) Pohl, R.; Socha, O.; Slavíček, P.; Šála, M.; Hodgkinson, P.; Dračínský, M. Proton transfer in guanine-cytosine base pair analogues studied by NMR spectroscopy and PIMD simulations. *Faraday Discuss.* **2018**, *212*, 331−344.
(58) McConnell, T. L.; Wetmore, S. D. How do size-expanded DNA nucleobases enhance duplex stability? Computational analysis of the hydrogen-bonding and stacking ability of xDNA bases. *J. Phys. Chem. B* **2007**, *111*, 2999−3009.
(59) Štoček, J. R.; Dračínský, M. Tautomerism of Guanine Analogues. *Biomolecules* **2020**, *10*, 170−179.
(60) Fan, W. J.; Zhang, R. Q.; Liu, S. B. Computation of large systems with an economic basis set: Structures and reactivity indices of nucleic acid base pairs from density functional theory. *J. Comput. Chem.* **2007**, *28*, 967−974.
(61) Wheaton, C. A.; Dobrowolski, S. L.; Millen, A. L.; Wetmore, S. D. Nitrosubstituted aromatic molecules as universal nucleobases: Computational analysis of stacking interactions. *Chem. Phys. Lett.* **2006**, *428*, 157−166.
(62) Šponer, J.; Leszczynski, J.; Hobza, P. Electronic properties, hydrogen bonding, stacking, and cation binding of DNA and RNA bases. *Biopolymers* **2001**, *61*, 3−31.
(63) Cabaj, M. K.; Dominiak, P. M. Frequency and hydrogen bonding of nucleobase homopairs in small molecule crystals. *Nucleic Acids Res.* **2020**, *48*, 8302−8319.
(64) Ranga, S.; Mukherjee, M.; Dutta, A. K. Interactions of Solvated Electrons with Nucleobases: The Effect of Base Pairing. *ChemPhysChem* **2020**, *21*, 1019−1027.
(65) Cuyacot, B. J. R.; Durník, I.; Foroutan-Nejad, C.; Marek, R. Anatomy of Base Pairing in DNA by Interacting Quantum Atoms. *J. Chem. Inf. Model.* **2021**, *61*, 211−222.
(66) Janeba, Z.; Holý, A.; Masojidkova, M. Synthesis of acyclic nucleoside and nucleotide analogs derived from 6-amino-7H-purin-8(9H)-one. *Collect. Czech. Chem. Commun.* **2000**, *65*, 1126−1144.
(67) McFarland, J. M.; Francis, M. B. Reductive alkylation of proteins using iridium catalyzed transfer hydrogenation. *J. Am. Chem. Soc.* **2005**, *127*, 13490−13491.
(68) Štoček, J. R.; Bártová, K.; Čechová, L.; Šála, M.; Socha, O.; Janeba, Z.; Dračínský, M. Determination of nucleobase-pairing free energies from rotamer equilibria of 2-(methylamino)pyrimidines. *Chem. Commun.* **2019**, *55*, 11075−11078.
(69) Kyogoku, Y.; Lord, R. C.; Rich, A. Effect of Substituents on Hydrogen Bonding of Adenine and Uracil Derivatives. *Proc. Natl. Acad. Sci. U. S. A.* **1967**, *57*, 250−257.
(70) Murray, T. J.; Zimmerman, S. C. New Triply Hydrogen-Bonded Complexes with Highly Variable Stabilities. *J. Am. Chem. Soc.* **1992**, *114*, 4010−4011.
(71) Hamilton, A. D.; Vanengen, D. Induced Fit in Synthetic Receptors - Nucleotide Base Recognition by a Molecular Hinge. *J. Am. Chem. Soc.* **1987**, *109*, 5035−5036.
(72) Jorgensen, W. L.; Pranata, J. Importance of Secondary Interactions in Triply Hydrogen-Bonded Complexes - guanine-cytosine vs uracil-2,6-diaminopyridine. *J. Am. Chem. Soc.* **1990**, *112*, 2008−2010.
(73) Papmeyer, M.; Vuilleumier, C. A.; Pavan, G. M.; Zhurov, K. O.; Severin, K. Molecularly Defined Nanostructures Based on a Novel AAA-DDD Triple Hydrogen-Bonding Motif. *Angew. Chem., Int. Ed.* **2016**, *55*, 1685−1689.
(74) Feng, Y. N.; Philp, D. A Molecular Replication Process Drives Supramolecular Polymerization. *J. Am. Chem. Soc.* **2021**, *143*, 17029−17039.
(75) Becke, A. D. Density-Functional Thermochemistry 3. The Role of Exact Exchange. *J. Chem. Phys.* **1993**, *98*, 5648−5652.
(76) Lee, C. T.; Yang, W. T.; Parr, R. G. Development of the Colle-Salvetti Correlation-Energy Formula into a Functional of the Electron-Density. *Phys. Rev. B* **1988**, *37*, 785−789.
(77) Barone, V.; Cossi, M. Quantum calculation of molecular energies and energy gradients in solution by a conductor solvent model. *J. Phys. Chem. A* **1998**, *102*, 1995−2001.
(78) Cossi, M.; Rega, N.; Scalmani, G.; Barone, V. Energies, structures, and electronic properties of molecules in solution with the C-PCM solvation model. *J. Comput. Chem.* **2003**, *24*, 669−681.
(79) Grimme, S.; Antony, J.; Ehrlich, S.; Krieg, H. A consistent and accurate ab initio parametrization of density functional dispersion

https://doi.org/10.1021/acsomega.3c03244
ACS Omega 2023, 8, 25538−25548

correction (DFT-D) for the 94 elements H-Pu. *J. Chem. Phys.* **2010**, *132*, 154104.
(80) Frisch, M. J.; Trucks, G. W.; Schlegel, H. B.; Scuseria, G. E.; Robb, M. A.; Cheeseman, J. R.; Scalmani, G.; Barone, V.; Petersson, G. A.; Nakatsuji, H.; Li, X.; Caricato, X.; Marenich, A. V.; Bloino, J.; Janesko, B. G.; Gomperts, R.; Mennucci, B.; Hratchian, H. P.; Ortiz, J. V.; Izmaylov, A. F.; Sonnenberg, J. L.; Williams-Young, D.; Ding, F.; Lipparini, F.; Egidi, F.; Goings, J.; Peng, B.; Petrone, A.; Henderson, T.; Ranasinghe, D.; Zakrzewski, V. G.; Gao, J.; Rega, N.; Zheng, G.; Liang, W.; Hada, M.; Ehara, M.; Toyota, K.; Fukuda, R.; Hasegawa, J.; Ishida, M.; Nakajima, T.; Honda, Y.; Kitao, O.; Nakai, H.; Vreven, T.; Throssell, K.; Montgomery, Jr., J. A.; Peralta, J. E.; Ogliaro, F.; Bearpark, M. J.; Heyd, J. J.; Brothers, E. N.; Kudin, K. N.; Staroverov, V. N.; Keith, T. A.; Kobayashi, R.; Normand, J.; Raghavachari, K.; Rendell, A. P.; Burant, J. C.; Iyengar, S. S.; Tomasi, J.; Cossi, M.; Millam, J. M.; Klene, M.; Adamo, C.; Cammi, R.; Ochterski, J. W.; Martin, R. L.; Morokuma, K.; Farkas, O.; Foresman, J. B.; Fox, D. J. *Gaussian 16, Revision A.03*; Gaussian, Inc.: Wallingford CT, 2016.

https://doi.org/10.1021/acsomega.3c03244
ACS Omega 2023, 8, 25538−25548